MTL neurons phase-lock to human hippocampal theta

Daniel R. Schonhaut[1], **Ashwin G. Ramayya**[2], **Ethan A. Solomon**[3], **Nora A. Herweg**[4], **Itzhak Fried**[5,6], **Michael J. Kahana**[4*]

*For correspondence:
kahana@psych.upenn.edu (MJK)

[1]Department of Neuroscience, Perelman School of Medicine, University of Pennsylvania, Philadelphia, PA 19104, USA; [2]Department of Neurosurgery, Hospital of the University of Pennsylvania, Philadelphia, PA 19104, USA; [3]Department of Bioengineering, University of Pennsylvania, Philadelphia, PA 19104, USA; [4]Department of Psychology, University of Pennsylvania, Philadelphia, PA 19104, USA; [5]Department of Neurosurgery, David Geffen School of Medicine and Semel Institute for Neuroscience and Human Behavior, University of California, Los Angeles, CA 90095, USA; [6]Tel-Aviv Medical Center and Sackler Faculty of Medicine, Tel-Aviv University, Tel-Aviv 69978, Israel

Abstract   Memory formation depends on neural activity across a network of regions, including the hippocampus and broader medial temporal lobe (MTL). Interactions between these regions have been studied indirectly using functional MRI, but the bases for inter-regional communication at a cellular level remain poorly understood. Here we evaluate the hypothesis that oscillatory currents in the hippocampus synchronize the firing of neurons both within and outside the hippocampus. We recorded extracellular spikes from 1,854 single- and multi-units simultaneously with hippocampal local field potentials (LFPs) in 28 neurosurgical patients who completed virtual navigation experiments. A majority of hippocampal neurons phase-locked to oscillations in the slow (2-4Hz) or fast (6-10Hz) theta bands, with a significant subset exhibiting nested slow theta × beta frequency (13-20Hz) phase-locking. Outside of the hippocampus, phase-locking to hippocampal oscillations occurred only at theta frequencies and primarily among neurons in the entorhinal cortex and amygdala. Extrahippocampal neurons phase-locked to hippocampal theta even when theta did not appear locally. These results indicate that spike-time synchronization with hippocampal theta is a defining feature of neuronal activity in the hippocampus and structurally-connected MTL regions. Theta phase-locking could mediate flexible communication with the hippocampus to influence the content and quality of memories.

Introduction

The hippocampus is the operational hub of a spatially distributed episodic memory system that enables us to remember past experiences in rich detail, together with the space and time that they occurred (*Eichenbaum, 2000*; *Moscovitch et al., 2016*). To serve in this capacity, the hippocampus must maintain precise but flexible connections with the rest of the memory system. Understanding the mechanisms that govern inter-regional connections among regions supporting episodic memory is a major concern of systems neuroscience, and progress in this area could accelerate efforts to develop treatments for memory disorders and age-related memory decline.

A leading hypothesis is that theta (2-10Hz) oscillations within the hippocampus facilitate interactions between the hippocampus and other brain regions (*Buzsáki, 2010*; *Fell and Axmacher, 2011*; *Moscovitch et al., 2016*). Hippocampal neurons are more receptive to synaptic excitation at spe-

42 cific theta phases (*Kamondi et al., 1998*), so well-timed inputs can more effectively drive activity
43 than inputs at random phases (*Fries, 2005*). Long-term potentiation and long-term depression in
44 the rodent hippocampus are also theta phase-dependent (*Pavlides et al., 1988*; *Huerta and Lis-*
45 *man, 1995*; *Hyman et al., 2003*), providing a putative link between the phase at which inputs arrive
46 and how strongly they are encoded. Experimental evidence for this hypothesis comes largely from
47 studies in the rat medial prefrontal cortex (mPFC), a downstream target of hippocampal area CA1.
48 mPFC neurons phase-lock to hippocampal theta during short-term memory tasks (*Siapas et al.,*
49 *2005*; *Hyman et al., 2005*; *Sirota et al., 2008*), and stronger phase-locking predicts better perfor-
50 mance (*Jones and Wilson, 2005*; *Hyman et al., 2010*; *Benchenane et al., 2010*; *Fujisawa and Buzsáki,*
51 *2011*) and greater information transfer between mPFC and hippocampal neurons (*Ito et al., 2018*;
52 *Padilla-Coreano et al., 2019*). Phase-locking to hippocampal theta is also prevalent among cells in
53 many other regions, including the entorhinal cortex (EC), amygdala, parietal cortex, thalamic nu-
54 cleus reuniens, and some subcortical and brainstem nuclei (*Kocsis and Vertes, 1992*; *Sirota et al.,*
55 *2008*; *Fujisawa and Buzsáki, 2011*; *Bienvenu et al., 2012*; *Fernández-Ruiz et al., 2017*; *Ito et al.,*
56 *2018*). Theta phase-synchronization could thus be a general mechanism for relaying information
57 between the hippocampus and a broad network of memory-related regions.
58   In humans, macroelectrode local field potential (LFP) recordings in epilepsy patients have re-
59 vealed sporadically-occurring theta oscillations in the hippocampus and cortex during spatial nav-
60 igation and episodic memory engagement (*Ekstrom et al., 2005*; *Watrous et al., 2011*; *Lega et al.,*
61 *2012*; *Watrous et al., 2013a*; *Zhang and Jacobs, 2015*; *Vass et al., 2016*; *Aghajan et al., 2017*; *Stangl*
62 *et al., 2021*). Studies relating theta power to memory have produced equivocal results (*Herweg*
63 *et al., 2020*), but macroscale theta phase-synchronization within the medial temporal lobe (MTL)
64 and PFC has consistently correlated with better memory performance (*Babiloni et al., 2009*; *Wa-*
65 *trous et al., 2013b*; *Solomon et al., 2017*; *Zheng et al., 2019*; *Kunz et al., 2019*). Considerably less is
66 known about how oscillations relate to neuronal firing in humans than in rodents. An early study
67 in epilepsy patients found that a large percentage of MTL and neocortical neurons phase-locked to
68 theta (among other frequency) oscillations in their local vicinity as subjects navigated through a vir-
69 tual environment (*Jacobs et al., 2007*), and another study discovered MTL neurons phase-locked
70 more strongly to locally-recorded theta oscillations while subjects viewed images that they later
71 recognized than those that they forgot (*Rutishauser et al., 2010*). These findings indicate that neu-
72 ral activity within the human episodic memory system is organized in part by a theta phase code.
73 However, oscillatory phase coding of neuronal responses outside the hippocampus have not been
74 well studied in humans, and the hypothesis that hippocampal theta facilitates inter-regional com-
75 munication lacks empirical validation. To address this question, we leveraged the rare opportunity
76 to record single- and multi-neuron activity simultaneously with LFP oscillations in multiple brain
77 regions, including the hippocampus, in 28 neurosurgical patients implanted with intracranial elec-
78 trodes.

79 ## Results
80 Subjects were implanted with depth electrodes in the hippocampus, EC, amygdala, parahippocam-
81 pal gyrus (PHG), superior temporal gyrus (STG), orbitofrontal cortex (OFC), and anterior cingulate
82 cortex (ACC). Using microwires that extended from the tips of these depth probes, we recorded ex-
83 tracellular spikes from 1,854 single- and multi-units (hereafter called 'neurons'; Table 1) as subjects
84 navigated through a virtual environment while completing one of several spatial memory tasks
85 whose data we pooled for this analysis (see Methods). In total, we identified 10-71 (median=30.0)
86 neurons per session across 55 recording sessions, and the firing rates of these neurons were log-
87 normally distributed (median=2.0Hz). In addition, every subject had at least one microwire bundle
88 implanted in the hippocampus, permitting neuronal firing to be analyzed simultaneously with os-
89 cillatory activity in the hippocampal LFP.

Identifying oscillations in hippocampal microwire LFPs

Existing studies that reported oscillatory properties of the human hippocampus during navigation have primarily utilized implanted macroelectrodes that integrate activity over hundreds of thousands of neurons (*Ekstrom et al., 2005*; *Watrous et al., 2011*, *2013a*; *Aghajan et al., 2017*; *Vass et al., 2016*). As microwires used in the present study record at far smaller spatial scales, we first considered whether comparable oscillatory properties are observed in microwires as in macroelectrode LFPs. We focused on 1-30Hz signals for this analysis, avoiding higher frequencies at which spike-related artifacts can complicate LFP interpretation (*Manning et al., 2009*; *Buzsáki et al., 2012*; *Ray, 2015*). Many individual electrodes showed peaks in spectral power that rose above the background 1/f line in session-averaged LFP spectrograms (Figure 1A), indicating the potential presence of oscillatory activity (*Donoghue et al., 2020*). The frequency and magnitude of these spectral peaks varied considerably across subjects (compare Figure 1A subpanels) yet were nearly exclusively observed between 2-20Hz.

To determine if spectral peaks were associated with sustained oscillations versus asynchronous, high-amplitude events, we used the BOSC (Better OSCillation) detection method to identify time-resolved oscillatory 'bouts' in each hippocampal microwire recording (*Whitten et al., 2011*). Briefly, BOSC (alternatively called 'P-episode') defines an oscillatory bout according to two threshold criteria, such that spectral power at a given frequency must exceed: (1) a statistically-defined amplitude above the 1/f spectrum, for (2) a minimum defined duration (we used 3 cycles; see Methods for more details). Figure 1B shows an example hippocampal LFP in which an initially aperiodic, '1/f-like' signal transitioned into a strong, 6Hz oscillation that persisted for 6 cycles, with the BOSC-defined oscillatory bout highlighted in pink.

Across subjects, hippocampal oscillatory bouts were present between ∼1-6% of the time at the examined frequencies (Figure 1C; Figure 1—figure supplement 5 shows oscillatory prevalence in other regions for comparison). The prevalence of these oscillations was not uniform across frequencies, but instead clustered around three, well-separated bands with peaks at 3Hz, 7Hz, and 15Hz, respectively. These frequencies are consistent with the hippocampal slow theta (alternatively 'delta'; 2-4Hz), fast theta (6-10Hz), and beta band rhythms (13-20Hz) previously described in macroelectrode recordings, and the prevalence of oscillatory bouts in our data was comparable to these earlier studies (*Ekstrom et al., 2005*; *Lega et al., 2012*; *Watrous et al., 2013a*; *Goyal et al., 2020*). Oscillatory prevalence varied between these frequency bands ($\chi^2(2) = 13.9$, $p < 0.0001$, likelihood ratio test between linear mixed-effects models testing frequency band as a fixed effect and holding subject as a random effect), such that slow theta appeared more prevalent than fast theta ($z = 2.4$, $p = 0.0336$, post-hoc pairwise z-tests, Bonferroni-Holm corrected for multiple comparisons) or beta ($z = 3.9$, $p = 0.0002$). Fast theta and beta oscillations occurred at similar rates ($z = 1.5$, $p = 0.1218$). These findings indicate that the human hippocampus exhibits several distinct, low frequency oscillations that are conserved across spatial scales spanning several orders of magnitude, from microwire to macroelectrode fields. Moreover, theta oscillations are the predominant oscillatory component of the hippocampal LFP during virtual navigation.

Individual neuron phase-locking to hippocampal oscillations

Having confirmed the presence of hippocampal theta and beta oscillations, we next asked how these oscillations interacted with the timing of neuronal firing throughout recorded regions (Table 1). We quantified the phase-locking strength of individual neurons to ipsilateral hippocampal oscillations at a range of frequencies from 1-30Hz. A neuron's phase-locking strength was defined as the mean resultant length (MRL) of hippocampal LFP phases across spike times at a given frequency, z-scored against a null distribution of MRLs obtained by circularly-shifting the neuron's spike train 10,000 times at random (see Methods). To control for the possibility that some neurons might phase-lock to asynchronous events in the hippocampal LFP, such as sharp waves or interictal discharges (*Skelin et al., 2021*; *Reed et al., 2020*), we restricted our analysis to spikes that coincided with BOSC-detected oscillatory bouts at each frequency, excluding 11% of neurons for which the

140 number of included spikes was insufficient to accurately gauge phase-locking (see Methods).

141 Figure 2A illustrates the phase-locking of an EC neuron whose spikes appear in raster format
142 above a simultaneously-recorded, 3s hippocampal LFP trace exhibiting slow theta rhythmicity. The
143 neuron fired in bursts of 2-8 spikes on a majority of theta cycles, with each burst generally aligned
144 with the theta cycle peak, while nearly no spikes occurred near the theta trough. Next, we exam-
145 ined the population phase-locking statistics for this neuron across the recording session (Figure 2C).
146 Computing the mean hippocampal LFP trace surrounding each spike (the 'spike-triggered average
147 LFP'), we confirmed that the neuron preferentially fired just after the theta peak, with synchronous
148 theta oscillations extending more than a full cycle before and after spike onset (Figure 2C, left sub-
149 panel, blue line). As a control, we also examined a spike-triggered average LFP drawn at random
150 from the null distribution, which showed a nearly flat line consistent with absent phase-locking
151 (Figure 2C, left subpanel, gray line). Graphing this neuron's phase-locking strength at frequencies
152 from 1-30Hz revealed that phase-locking to hippocampal oscillations occurred only in the slow
153 theta band, peaking at 3Hz (Figure 2C, middle subpanel). Finally, the circular histogram of spike-
154 coincident, 3Hz hippocampal LFP phases showed that most spikes occurred within a quarter-cycle
155 after the theta peak (Figure 2C, right subpanel). Figure 2B and D-J applies this analysis to represen-
156 tative neurons in the hippocampus, EC, amygdala, and OFC that phase-locked to LFP oscillations
157 in the hippocampus. We observed that most neurons exhibited unimodal peaks in phase-locking
158 strength, most commonly in the theta range.

Regional differences in hippocampal phase-locking

160 We next examined phase-locking at the population level, first considering the percentage of neu-
161 rons in each region that significantly phase-locked to ipsilateral hippocampal LFP oscillations, ir-
162 respective of frequency. For each neuron, we derived an empirical phase-locking p-value by com-
163 paring the neuron's maximum phase-locking strength, across frequencies, to its null distribution
164 of maximum phase-locking strengths (see Methods). We then applied false discovery rate (FDR)
165 correction at $\alpha = 0.05$ to the distribution of p-values within each region. Finally, for each region out-
166 side the hippocampus, we performed the same analyses and statistical corrections with respect
167 to LFP oscillations in each neuron's local region (proximal to the electrode where a neuron was
168 recorded). This last step allowed us to directly compare phase-locking rates to local versus remote
169 hippocampal influences.

170 Figure 3A illustrates these analyses. As expected, neurons within the hippocampus phase-
171 locked to hippocampal oscillations at the highest rate among recorded regions, with 59% of hip-
172 pocampal neurons being significantly phase-locked after FDR-correction. High phase-locking rates
173 to the hippocampus were also found for neurons in the EC (41%) and amygdala (29%), with phase-
174 locking rates in the EC being significantly higher than those in the amygdala ($z = 3.6$, $p = 0.0004$,
175 post-hoc pairwise z-test from a logistic mixed-effects model testing neuron region as a fixed ef-
176 fect and holding subject as a random effect). Whereas amygdala neurons phase-locked to local
177 oscillations at significantly higher rates (46%) than to oscillations in the hippocampus ($\chi^2(1) = 32.6$,
178 $p < 0.0001$), neurons in the EC phase-locked to local (40%) and hippocampal oscillations at indistin-
179 guishable rates ($\chi^2(1) = 0.2$, $p = 0.6672$) (likelihood ratio tests between logistic mixed-effects models
180 testing oscillation region as a fixed effect and holding subject as a random effect).

181 These results stood in stark contrast to all remaining regions, where phase-locking to the hip-
182 pocampus occurred at rates below 5%. Phase-locking to local oscillations was nonetheless preva-
183 lent in the PHG (24%) and STG (49%), indicating that many of these neurons were rhythmically
184 entrained, just not by oscillations in the hippocampus. In two regions of the prefrontal cortex, lo-
185 cal phase-locking rates were relatively low (16% of OFC neurons and 6% of ACC neurons) although
186 still significantly higher than phase-locking rates to the hippocampus (OFC: $\chi^2(1) = 20.9$, $p < 0.0001$;
187 ACC: $\chi^2(1) = 5.6$, $p = 0.0178$; likelihood ratio tests between logistic mixed-effects models, as above).
188 Altogether, these results highlight a triad of regions in the hippocampus, EC, and amygdala with
189 strong spike-time synchronization to hippocampal oscillations, while neurons in more remote, cor-

190 tical regions known to interact with hippocampal-dependent processes (*Eichenbaum, 2000*; *Squire,*
191 *2011*; *Ranganath and Ritchey, 2012*) were minimally entrained by hippocampal rhythms.

Frequencies of hippocampal phase-locking

193 Individual neuron examples suggested that phase-locking to the hippocampus occurred most com-
194 monly at theta frequencies (Figure 2), although our analysis of hippocampal LFPs revealed oscilla-
195 tions extending up to ~20Hz (Figure 1). Does this observation of preferential theta phase-locking
196 hold at the population level, and does the frequency of hippocampal phase-locking vary by a
197 neuron's region-of-origin? To answer these questions, we generated heatmaps of phase-locking
198 strength by frequency for all neurons that phase-locked significantly to hippocampal oscillations
199 at *any* frequency, as defined in the previous section (Figure 3B; these neurons correspond to the
200 dark gray bars in Figure 3A). We made separate heatmaps for neurons in the hippocampus, EC,
201 amygdala, and remaining regions, respectively, sorting the neurons in each region by frequency of
202 maximum phase-locking strength. Figure 3—figure supplement 1 shows analogous heatmaps for
203 neurons in each region with respect to local, rather than hippocampal, oscillations (matching the
204 light gray bars in Figure 3A).

205 In the hippocampus, neurons phase-locked to local oscillations predominately between 2-20Hz.
206 Only a few neurons phase-locked weakly at higher frequencies, which may be largely attributable
207 to false discoveries (Figure 3B, far-left subpanel). Within the 2-20Hz range, phase-locking was not
208 unimodal, but instead clustered around three distinct peaks in the slow theta, fast theta, and beta
209 bands. Most hippocampal neurons phase-locked to only a single band, with the exception of neu-
210 rons that phase-locked maximally to beta oscillations, which also showed a near-universal ten-
211 dency to phase-lock strongly to slow theta (see for example Figure 2H). These neurons may best
212 be classified as nested slow theta × beta phase-locking neurons, which to our knowledge have not
213 previously been reported. In contrast, we did not observe nested phase-locking between fast theta
214 and beta oscillations or between any other pair of frequency bands.

215 Among neurons outside the hippocampus, phase-locking to hippocampal oscillations occurred
216 within a more constrained frequency range, between 2-10Hz (Figure 3B, left three subpanels). In
217 the EC, similar numbers of neurons showed preferential phase-locking to slow and fast hippocam-
218 pal theta, respectively. In the amygdala and remaining cortical regions, this balance shifted: only
219 a few neurons phase-locked to fast hippocampal theta, while most neurons were entrained exclu-
220 sively by slow theta. Thus, while hippocampal neurons phase-locked to both theta and beta bands,
221 for neurons outside the hippocampus, spike-time synchronization with hippocampal oscillations
222 was restricted to theta frequencies.

223 We confirmed these conclusions in a secondary analysis that examined the mean phase-locking
224 strength at each frequency across all neurons in each region, regardless of individual phase-locking
225 significance (Figure 3C). This approach benefited from not requiring an explicit significance thresh-
226 old to be defined. Instead, we assumed that if the neurons in a given region *did not* phase-lock mea-
227 surably to the hippocampus, then the mean phase-locking strength across these neurons would
228 approach zero (no difference versus the null distribution) at increasing sample size. Indeed, popu-
229 lation phase-locking strengths were close to zero across frequencies for neurons in the PHG, STG,
230 OFC, and ACC, consistent with the relative absence of individually phase-locked neurons in these
231 regions. In contrast, neurons in the EC and amygdala both showed strong phase-locking to slow
232 hippocampal theta frequencies, while EC but not amygdala neurons exhibited a secondary rise in
233 phase-locking strength to fast hippocampal theta. Finally, neurons in the hippocampus showed
234 stronger phase-locking to hippocampal oscillations at all frequencies than neurons in any other re-
235 gion, with peaks in phase-locking strength at all three (slow theta, fast theta, and beta) oscillatory
236 bands.

Local oscillation effects on remote hippocampal phase-locking

Our data reveal that neurons not only within the hippocampus, but in remote regions – particularly the entorhinal cortex and amygdala – are entrained by hippocampal theta phase. How do these remote spike-phase associations occur? One possibility, given the strength of phase-locking to local oscillations (Figure 3—figure supplement 1), is that phase-locking to the hippocampus is an indirect phenomenon, facilitated by transient phase coupling between oscillations in different regions (Figure 4—figure supplement 1, blue arrows). In rodents, however, neurons in some regions phase-lock to hippocampal theta even in the absence of a local theta rhythm (*Siapas et al., 2005*), suggesting that inter-regional oscillatory coupling is not a strict requirement for remote spike-phase associations to occur (Figure 4—figure supplement 1, red arrow).

To examine how inter-regional oscillatory coupling contributed to remote spike-phase associations, we first considered the co-occurrence of oscillatory bouts in the hippocampus and in each extrahippocampal region. We reasoned that if remote spike-phase associations were mediated by oscillatory coupling, then regions where neurons phase-locked to the hippocampus at higher rates should also show higher levels of oscillatory co-occurrence. Consistent with this hypothesis, hippocampal oscillations overlapped more with oscillations in the EC and amygdala than with oscillations in the STG, OFC, and ACC at most frequencies (Figure 4A; overlap calculated using the Dice similarity coefficient). However, hippocampal and PHG oscillations also overlapped strongly despite the relative absence of PHG neuron phase-locking to the hippocampus (Figure 3A) and abundant PHG neuron phase-locking to local theta (Figure 3—figure supplement 1). Moreover, the overlap between local and hippocampal oscillations never exceeded 20% in any region at any frequency, indicating that neurons could, in principle, phase-lock to hippocampal oscillations independent of local oscillations, and vice versa. Altogether these results provide a mixed view for the hypothesis that inter-regional oscillatory coupling and remote spike-phase associations are interchangeable.

Next, we directly compared how remote phase-locking to the hippocampus varied as a function of local phase-locking effects. For each extrahippocampal neuron, we subdivided spikes into two categories: (1) spikes that occurred when an oscillation was present in *both* the hippocampus and a neuron's local region, and (2) spikes that occurred when an oscillation was present in the hippocampus but *not* the neuron's local region. As chance-level phase-locking values are sample size dependent, for each neuron we matched the number of spikes in each group, at each frequency, excluding neurons with insufficient sample size (<50 spikes at any frequency; see Methods). We then applied the same methods for determining phase-locking strength and significance as described in the previous section.

Figure 4B shows the results from these analyses. FDR-corrected phase-locking rates during co-occurring local and hippocampal oscillations were comparable to phase-locking rates when all spikes were included (see Figure 3A), with high phase-locking to hippocampal oscillations occurring among neurons in the EC and amygdala and minimal phase-locking among neurons in other regions. In contrast, when hippocampal oscillations occurred without co-occurring local oscillations, phase-locking rates to the hippocampus declined by nearly two-thirds in the EC (from 39% of neurons to 14%) and by half in the amygdala (from 28% to 15%), while phase-locking to the hippocampus in other regions mostly vanished. Phase-locking strength to the hippocampus decreased specifically at theta frequencies, and even neurons that remained significantly phase-locked in the absence of local oscillations showed reduced phase-locking strength (Figure 4C). We also considered the reverse analysis, asking whether phase-locking to local oscillations depended on the presence of co-occurring oscillations in the hippocampus. While local phase-locking rates in the amygdala and neocortex were unaffected by hippocampal oscillation presence, in the EC the percentage of locally phase-locked neurons was reduced by more than half when hippocampal oscillations were absent (Figure 4—figure supplement 2).

Finally, we confirmed these findings at the population level by computing the mean phase-

287 locking strength across all neurons in each region, without regard to phase-locking significance,
288 while still matching the number of spikes at each frequency between conditions in which local and
289 hippocampal oscillations co-occurred versus only hippocampal oscillations occurred. As in Figure
290 3C, when local and hippocampal oscillations co-occurred, EC and amygdala neurons both phase-
291 locked strongly to slow hippocampal theta, phase-locking to fast hippocampal theta was restricted
292 to EC neurons, and other regions showed negligible phase-locking to hippocampal oscillations at
293 any frequency (Figure 4D, left subpanel). When local theta was absent, the strength of EC and
294 amygdala neuron phase-locking to hippocampal theta was reduced by half, while still remaining
295 well above chance (Figure 4D, right subpanel). Collectively, these results provide direct evidence
296 that inter-regional LFP-LFP theta coupling augments but is not strictly required for extrahippocam-
297 pal neuron phase-locking to hippocampal theta.

Discussion

299 By combining datasets of single- and multi-neuron recordings in human subjects, we provide an
300 empirical test of the hypothesis that LFP oscillations in the hippocampus synchronize the timing
301 of neuronal firing both within the hippocampus and in functionally associated regions. Consis-
302 tent with prior studies, we identify sporadic, oscillatory bouts in hippocampal LFPs within slow
303 theta (2-4Hz), fast theta (6-10Hz), and beta (13-20Hz) bands while subjects engaged in virtual nav-
304 igation. Individual hippocampal neurons phase-lock to oscillations in each of these bands, includ-
305 ing a previously undiscovered group of neurons that phase-lock to nested slow theta and beta
306 rhythms. Outside the hippocampus, phase-locking to hippocampal oscillations occurs in both a
307 regionally-specific (primarily EC and amygdala neurons) and frequency-specific (theta frequency
308 preferring) manner. We further show a dissociation between region and frequency in the selective
309 phase-locking of EC neurons to fast hippocampal theta, whereas neurons in all regions outside
310 the hippocampus show some level of phase-locking to slow hippocampal theta. Finally, we pro-
311 vide the first direct evidence in humans that LFP-LFP coupling enhances spike-time synchroniza-
312 tion between regions, as extrahippocampal neurons phase-lock approximately twice as strongly
313 to hippocampal theta during co-occurring local theta oscillations versus when local theta is absent.
314 Taken together, these findings reveal a fundamental relationship between MTL neuron firing and
315 hippocampal theta phase that underscores a hypothesized role for theta oscillations in routing the
316 information contents of memory.

317 We note a particularly striking difference between phase-locking rates to hippocampal theta in
318 the EC and amygdala (∼30-40% of neurons) relative to all other recorded regions, which phase-lock
319 minimally (<5%) despite their associations with hippocampal-dependent processes (*Eichenbaum,*
320 *2000*; *Squire, 2011*; *Ranganath and Ritchey, 2012*). This result is consistent with structural anatomy,
321 as the hippocampus maintains strong, reciprocal connections with the EC and amygdala while
322 connections to neocortex are sparser (*Amaral, 2011*). Still, given evidence in rodents that some
323 mPFC neurons project directly to the hippocampus (*Rajasethupathy et al., 2015*), phase-lock to
324 hippocampal theta (*Siapas et al., 2005*; *Hyman et al., 2005*; *Sirota et al., 2008*; *Ito et al., 2018*;
325 *Padilla-Coreano et al., 2019*), and are critical for memory retrieval (*Rajasethupathy et al., 2015*;
326 *Yadav et al., 2022*), we expected that ACC and OFC neurons would show stronger associations with
327 hippocampal theta than we observed. One possibility is that strong phase-locking to hippocampal
328 theta occurs in the EC and amygdala by default, whereas phase-locking among neurons in the
329 mPFC and other cortical areas is task-dependent. Consistently, a recent study in humans found
330 that ACC and pre-supplementary motor area neurons phase-locked to hippocampal theta during
331 a task-switching experiment in which subjects alternated between making recognition memory-
332 based or categorization-based decisions (*Minxha et al., 2017*). To the best of our knowledge, this
333 is the only other study that has reported extrahippocampal phase-locking to hippocampal theta
334 in humans, although it will be interesting for future work to consider how phase-locking rates vary
335 by region under different task and stimulus conditions.

336 We find two differences in hippocampal phase-locking properties between the EC and amyg-
337 dala. First, as in neocortical regions, amygdala neurons phase-lock at higher rates to local than
338 hippocampal oscillations, and local and hippocampal phase-locking occur at least somewhat in-
339 dependently. By contrast, EC neurons phase-lock to local and hippocampal theta oscillations at
340 indistinguishable rates, and phase-locking is greatly disrupted when EC and hippocampal theta
341 bouts are out of sync. It is worth noting that in rodents, EC and hippocampal theta are phase-
342 shifted but otherwise largely interchangeable, with EC inputs playing a major role in hippocampal
343 theta generation *Buzsáki* (*2002*). Theta phase synchronization between these regions is critical
344 to explain many circuit-level phenomena in rodents, including grid cell and place cell interactions,
345 phase precession, and encoding/retrieval phase separation *O'Keefe and Burgess* (*2005*); *Hasselmo*
346 (*2005*); *Burgess et al.* (*2007*); *Bonnevie et al.* (*2013*); *Fernández-Ruiz et al.* (*2017*). Theta occurs more
347 sporadically in humans and other primates than in rodents, and may differ between mammals in
348 other ways not yet well understood (*Eliav et al., 2018*; *Trimper and Colgin, 2018*; *Bush and Burgess,*
349 *2019*). Still, our results indicate that as in rodents, EC and hippocampal neurons in humans retain
350 a uniquely high degree of spike-time synchronization with an overlapping theta rhythm.

351 The second difference between EC and amygdala neurons concerns the frequency of hippocam-
352 pal phase-locking, with neurons in both regions phase-locking to slow hippocampal theta but only
353 EC neurons phase-locking measurably to fast theta. This result may be placed in context with recent
354 observations that hippocampal theta frequency varies along the longitudinal axis of the hippocam-
355 pus, with faster theta occurring more posteriorly (*Goyal et al., 2020*; *Penner et al., 2022*), where
356 the density of EC relative to amygdalar afferents is greater (*Strange et al., 2014*). While most of our
357 hippocampal electrodes were located anteriorly and precluded a direct analysis of EC and amyg-
358 dala phase-locking by hippocampal electrode position, this hypothesis may be worth examining in
359 a different dataset.

360 We note an important difference in our methodological approach compared to prior studies
361 that examined spike-LFP phase relations in humans (*Jacobs et al., 2007*; *Rutishauser et al., 2010*;
362 *Watrous et al., 2018*; *Kamiński et al., 2020*; *Minxha et al., 2020*; *Qasim et al., 2021*). These studies
363 typically analyzed either all spikes or a large majority of spikes during time windows of interest,
364 sometimes excluding spikes when spectral power fell below a predefined threshold, e.g. the bot-
365 tom 25th percentile. Here we wished to strictly test the hypothesis that neurons phase-lock to
366 neural *oscillations* in the hippocampus, as defined by intervals when spectral power exceeds the
367 1/f spectrum by a significant amount for a sustained duration (*Whitten et al., 2011*; *Donoghue*
368 *et al., 2022*). We considered this approach especially important given the sporadic nature of oscil-
369 latory bouts in human LFP recordings and the prevalence of asynchronous, high power artifacts—
370 interictal discharges (*Reed et al., 2020*), sharp-wave ripples (*Skelin et al., 2021*), duplicate spikes
371 across channels (*Dehnen et al., 2021*), and movement or other non-neural artifacts that escape
372 algorithmic detection. In our experience, phase-locking analyses that did not restrict spikes to ver-
373 ified oscillations produced qualitatively similar group-level results as we report here, but included
374 many individual cases of likely spurious phase-locking to non-oscillatory signals. This methodologi-
375 cal difference might explain discrepancies between our results and earlier findings that hippocam-
376 pal neurons phase-lock to local oscillations at a wider range of frequencies, e.g. 20-30Hz, that we
377 did not observe (*Jacobs et al., 2007*).

378 This study has several important limitations. First, all subjects had pharmacoresistant epilepsy,
379 and we cannot rule out that some results might stem from pathological activity. However, we
380 sought to reduce this potential by analyzing spikes only during oscillatory bouts, and we are en-
381 couraged by the general agreement between our results and those in rodents. A second limitation
382 concerns the quality of unit isolation, as we recorded spikes from single microwires with limited
383 ability to resolve spiking contributions from different neurons. Although some studies in humans
384 have attempted to distinguish between single-units and multi-units and between excitatory and
385 inhibitory neurons, unit quality metrics from microwires do not leave us with high confidence in
386 the accuracy with which these distinctions can be made, while the potential for better quality unit

recordings using tetrodes or Neuropixels may soon provide clarity with respect to cell-type-specific differences (*Despouy et al., 2020*; *Chung et al., 2022*). In the meantime, we believe it is unlikely that this limitation would change any of our main conclusions, which do not depend on knowing if a unit is truly "single" versus a combination of several neighboring cells.

Still little is known about the relations between theta phase-locking and human cognition. Prior studies have focused on the behavioral correlates of phase-locking to local theta rhythms within the MTL; for example, successful image encoding was found to depend on theta phase-locking strength among hippocampal and amygdala neurons (*Rutishauser et al., 2010*), while another study found that MTL neurons can represent contextual information in their theta firing phase (*Watrous et al., 2018*). Here we show that hippocampal theta oscillations also inform the timing of neuronal firing in regions beyond the hippocampus, positioning theta oscillations at the interplay between local circuit computations and inter-regional communication. It remains unknown if behavioral or brain-state dissociations can be found between local and inter-regional phase-locking, or between spike-LFP and LFP-LFP phase synchronization. Such analyses could be well positioned to unite findings from animal and human studies and advance a more mechanistic account of hippocampal-dependent processes across multiple levels of scale, from single neurons to macroscopic fields.

Methods

Participants

Subjects were 28 patients with pharmacoresistant epilepsy who were implanted with depth electrodes to monitor seizure activity. Clinical teams determined the location and number of implanted electrodes in each patient. We performed bedside cognitive testing on a laptop computer. All testing was completed under informed consent. Experiments were approved by institutional review boards at the University of California, Los Angeles and the University of Pennsylvania.

Spatial navigation tasks

We analyzed data from 55 recording sessions (1-4 sessions per subject, mean duration = 33.6min). During each session, subjects played one of several first-person navigation games in which they freely explored a virtual environment and retrieved objects or navigated to specific locations. The details of these experiments have been previously described (*Ekstrom et al., 2003*; *Jacobs et al., 2010*; *Schonhaut et al., 2022*); for the purposes of the present study, we pooled data across these studies to generate a large sample for conducting electrophysiological analyses. We analyzed intervals in which subjects could freely navigate through the virtual environment.

Recording equipment

Each subject was implanted with six to 12 Behnke-Fried depth electrodes that feature macroelectrode contacts for clinical monitoring and 40μm diameter, platinum-iridium microwires for measuring microscale local field potentials (LFPs) and extracellular action potentials (*Fried et al., 1999*). Electrode localizations were confirmed by the clinical team using post-operative structural MRIs or post-operative CT scans co-registered to pre-operative structural MRIs. Microwires were packaged in bundles of eight high-impedance recording wires and one low-impedance wire that served as the recording reference. Each microwire bundle was threaded through the center of a depth probe and extended 5mm from the implanted end. As microwires splay out during implantation and cannot reliably be visualized on post-operative scans, electrode localizations are regarded with a ~5mm radius of uncertainty that preclude analyses at the level of regional substructures or hippocampal layers or subfields. Microwire LFPs were amplified and sampled at 28-32kHz on a Neuralynx Cheetah (Neuralynx, Tucson, AZ) or Blackrock NeuroPort (Blackrock Microsystems, Salt Lake City, UT) recording system.

Spike-sorting

We performed semi-automatic spike sorting and quality inspection on each microwire channel using the WaveClus software package in Matlab (*Quiroga et al., 2004*), as previously described (*Ekstrom et al., 2003*; *Schonhaut et al., 2022*). We isolated 0-8 units on each microwire channel, retaining both single-units and multi-units for subsequent analysis while removing units with low amplitude waveforms relative to the noise floor, non-neuronal shapes, inconsistent firing across the recording session, or other data quality issues. Spikes that clustered into separate clouds in reduced dimensional space were retained as separate units, while spikes that clustered into single clouds were merged. Repeated testing sessions occurred on different days, and we spike-sorted and analyzed these data separately.

LFP preprocessing and spectral feature extraction

Microwire LFPs were downsampled to 1000Hz, bandpass filtered between 0.1-80Hz using a zero-phase Hann window, and notch-filtered at 60Hz to remove electrical line noise. Bandpass frequencies were selected to reduce signal drift at the low end and spike waveform artifacts (or other high-amplitude noise) at the high end, while maintaining sufficient distance from frequencies of interest for analysis. Lastly, we identified and removed a small number of dead or overly noisy channels, identified as those for which the mean, cross-frequency spectral power differed by >2 standard deviations from the mean spectral power across channels in each microwire bundle. The remaining LFP channels were manually inspected prior to further analysis as a secondary quality inspection step. Lastly, we extracted instantaneous spectral power and phase estimates for each preprocessed LFP channel by convolving the time domain signal with 5-cycle complex wavelets at 30 frequencies, linearly-spaced from 1-30Hz.

Oscillatory bout identification

For each LFP channel, we identified time-resolved oscillatory bouts at the 30 frequencies defined in the previous section using the BOSC (Better OSCillation) detection method, as described previously (*Whitten et al., 2011*). BOSC defines an oscillatory bout according to two threshold criteria: a power threshold, P_T, and a duration threshold, D_T. P_T is set to the 95th percentile of the theoretical χ^2 probability distribution of power values at each frequency, under the null hypothesis that powers can be modeled as a straight power law decaying function (the '1/f' spectrum). Defining P_T for each frequency of interest requires first finding a best fit for 1/f. We obtained this fit by implementing the recently-developed FOOOF (Fitting Oscillations & One-Over F) algorithm, which uses an iterative fitting procedure to decompose the power spectrogram into oscillatory components and a 1/f background fit (*Donoghue et al., 2020*). To avoid assuming that the 1/f spectrum was stationary across the recording session, we divided the LFP into 30s epochs and re-fit 1/f (and P_T, by extension) in each epoch. Finally, we set $D_T = 3/f$, consistent with the convention used in previous studies (*Ekstrom et al., 2005*; *Watrous et al., 2011*; *Aghajan et al., 2017*), such that power at a given frequency f must exceed P_T for a minimum of 3 cycles for an oscillatory bout to be detected.

Oscillatory prevalence was calculated within three frequency bands of interest, defined as slow theta (2-4Hz), fast theta (6-10Hz), and beta (13-20Hz). For each subject, we calculated the average oscillatory bout percentage across recording sessions, hippocampal microwire channels, and frequencies within each band. The resulting matrix provided a single measure of hippocampal LFP oscillation prevalence within each band, from each subject. Differences between bands were assessed using a linear mixed-effects model to account for repeated samples within-subject.

Phase-locking strength and significance

We computed phase-locking strengths at 30 frequencies (1-30Hz with 1Hz spacing) between each neuron's spike times and oscillations in the hippocampus, as well as between each neuron's spike times and oscillations in the neuron's local region (other microwires in the same bundle, excluding

480 the neuron's own recording wire due to spike contamination of the LFP). For both of these com-
481 parisons, we retained only spikes that coincided with BOSC-detected oscillatory bouts to avoid
482 reporting spike-phase associations with non-oscillatory LFP phenomena. Phase-locking strength
483 was then calculated as follows: First, we calculated the mean resultant length (MRL) of hippocam-
484 pal LFP phases across spike times at each frequency, respectively. The MRL is equal to the sum
485 of phase angle unit vectors divided by the total number of samples, yielding a measure from 0 to
486 1 that indicates the extent to which the phase distribution is unimodal. This metric is sample size
487 dependent, with low n yielding artificially high MRLs due to chance clustering of phases. For this
488 reason, we excluded neurons with <50 spikes at all frequencies of interest. Several other factors
489 can artificially inflate the MRL, including nonuniform phase distributions in an underlying LFP sig-
490 nal, or autocorrelated spike times (*Siapas et al., 2005*). To control for these potential confounds,
491 we used a permutation-based procedure in which we circularly-shifted each neuron's spike train
492 at random and then recalculated MRLs at each frequency, repeating this process 10,000 times per
493 neuron to generate a null distribution. We then calculated phase-locking strength as the true MRL
494 at each frequency z-scored against null distribution MRLs at the corresponding frequencies.

495 To determine which neurons phase-locked significantly to local and hippocampal oscillations,
496 respectively, we calculated an empirical p-value for each neuron by comparing its maximum phase-
497 locking strength across frequencies to its null distribution of maximum phase-locking strengths,
498 using the formula $p = \frac{r+1}{n+1}$, where r is the number of permuted values $\geq$ the true value for a given
499 test statistic, and n is the total number of permutations (*North et al., 2002*). Finally, we false dis-
500 covery rate (FDR)-corrected p-values using the adaptive linear step-up procedure, which controls
501 the expected proportion of true null hypotheses among rejected nulls for both independent and
502 positively-dependent test statistics, and has greater statistical power than the commonly used
503 Benjamini-Hochberg procedure (*Benjamini et al., 2006*). FDR correction was applied separately to
504 p-values from each neuron region $\times$ LFP region (local or hippocampal) pair to control the expected
505 proportion of false positives within each of these groups. Neurons with FDR-corrected $p < 0.05$
506 were deemed significantly phase-locked.

Inter-regional oscillatory co-occurrence

508 Co-occurrence rates were determined between hippocampal and extrahippocampal oscillatory
509 bouts by quantifying the Dice coefficient between each hippocampal electrode and each ipsilateral,
510 extrahippocampal electrode. The Dice coefficient measures the similarity from 0 to 1 between two
511 sets A and B, with 0 indicating that the sets do not overlap and 1 indicating that A and B are equal:
512 $Dice = \frac{2|A \cap B|}{|A|+|B|}$, where $|A|$ and $|B|$ correspond to the number of elements in each set and $|A \cap B|$ is
513 the number of elements common to both sets. We calculated these values using binarized oscilla-
514 tion detection vectors (oscillation present or absent) as defined in "Oscillatory bout identification,"
515 separately at each 1-30Hz frequency.

Phase-locking to hippocampal oscillations during co-occurring or absent local os-cillations

518 We divided spikes from each extrahippocampal neuron into two groups according to the follow-
519 ing criteria: (1) BOSC-detected oscillations were present in both the hippocampus and a neuron's
520 local region, or (2) BOSC-detected oscillations were present in the hippocampus but not the neu-
521 ron's local region (Figure 4). These spike subsets were determined separately for each 1-30Hz
522 frequency. Phase-locking strengths were then calculated separately within each spike group, at
523 each frequency, and significance determined relative to null distributions as described in "Phase-
524 locking strength and significance." As chance-level phase-locking values are sample size dependent,
525 for each neuron we matched the number of spikes in each group, at each frequency, excluding
526 neurons with insufficient sample size (<50 spikes at any frequency). For example, for neuron i at
527 frequency j, if 200 spikes occurred when local and hippocampal oscillations were both present and
528 150 spikes occurred when only hippocampal oscillations were present, we selected 150 spikes from

529 the first group at random and proceeded to calculate phase-locking strength in each group. The

530 same analytical approach was applied to a supplemental analysis (Figure 4—figure supplement 2

531 in which extrahippocampal spikes were subdivided as: (1) local and hippocampal oscillations were

532 both present, or (2) local oscillations were present but hippocampal oscillations were absent.

Statistics

534 Linear and logistic mixed-effects models with fixed slopes and random intercepts were performed

535 using the lme4 package in R (*Baayen et al., 2008*). All models included a single random effect of

536 subject and a single fixed effect of interest, as stated in each result. p-values were obtained from

537 likelihood ratio tests between nested models (with versus without including the fixed effect). We

538 adopted this approach to control for inter-subject differences in our data that would be overlooked

539 when using conventional methods, like linear regression, that assume independence between neu-

540 rons. This approach was particularly important for comparing effects between regions, as each

541 subject had electrodes placed in only a subset of the regions that we analyzed. For models in

542 which the independent variable was a categorical measure with three or more levels, if the likeli-

543 hood ratio test revealed a significant effect ($p < 0.05$), we performed post-hoc, pairwise z-tests on

544 the fitted model terms with Bonferonni-Holm correction for multiple comparisons where noted in

545 the Results.

Software

547 Mixed-effects models were fit using the lme4 package in R (*Baayen et al., 2008*). Spike-sorting was

548 performed using the WaveClus software package in Matlab (*Quiroga et al., 2004*). All additional

549 analyses were performed, and plots generated, using code that was developed in-house in Python

550 3, utilizing standard libraries and the following, publicly-available packages: astropy, fooof, mat-

551 plotlib, mne, numpy, pandas, seaborn, scipy, statsmodels, and xarray.

Data availability

553 The data used in this study is publicly available for download from the Cognitive Electrophysiol-

554 ogy Data Portal (http://memory.psych.upenn.edu/Electrophysiological_Data). This dataset includes

555 de-identified, raw EEG data; spike-sorted unit data; and pre-processed phase-locking data. All data

556 analysis code and JupyterLab notebooks can be freely downloaded at the public GitHub repository:

557 https://github.com/dschonhaut/phase_locking.

Author Contributions

564 D.R.S. and M.J.K. designed the experiments. IF performed surgical procedures and supervised

565 recordings and data collection. D.R.S. analyzed the data. D.R.S. wrote the manuscript with feed-

566 back from all authors.

Competing Interests

568 The authors declare no competing interests.

References

570 **Aghajan ZM**, Schuette P, Fields TA, Tran ME, Siddiqui SM, Hasulak NR, Tcheng TK, Eliashiv D, Mankin EA, Stern

571 J, Fried I, Suthana N. Theta oscillations in the human medial temporal lobe during real-world ambulatory

572 movement. Curr Biol. 2017; 27(24):3743–3751.e3. doi: 10.1016/j.cub.2017.10.062.

573 **Amaral DG**. Memory: Anatomical organization of candidate brain regions. In: *Comprehensive Physiology* John
574 Wiley Sons, Ltd; 2011.p. 211–294. doi: 10.1002/cphy.cp010507.

575 **Baayen RH**, Davidson DJ, Bates DM. Mixed-effects modeling with crossed random effects for subjects and
576 items. Journal of Memory and Language. 2008; 59(4):390–412. doi: 10.1016/j.jml.2007.12.005.

577 **Babiloni C**, Vecchio F, Mirabella G, Buttiglione M, Sebastiano F, Picardi A, Di Gennaro G, Quarato PP, Grammaldo
578 LG, Buffo P, Esposito V, Manfredi M, Cantore G, Eusebi F. Hippocampal, amygdala, and neocortical synchro-
579 nization of theta rhythms is related to an immediate recall during Rey auditory verbal learning test. Hum
580 Brain Mapp. 2009; 30(7):2077–2089. doi: 10.1002/hbm.20648.

581 **Benchenane K**, Peyrache A, Khamassi M, Tierney PL, Gioanni Y, Battaglia FP, Wiener SI. Coherent theta oscil-
582 lations and reorganization of spike timing in the hippocampal-prefrontal network upon learning. Neuron.
583 2010; 66(6):921–936. doi: 10.1016/j.neuron.2010.05.013.

584 **Benjamini Y**, Krieger AM, Yekutieli D. Adaptive linear step-up procedures that control the false discovery rate.
585 Biometrika. 2006; 93(3):491–507. doi: 10.1093/biomet/93.3.491.

586 **Bienvenu TCM**, Busti D, Magill PJ, Ferraguti F, Capogna M. Cell-type-specific recruitment of amygdala in-
587 terneurons to hippocampal theta rhythm and noxious stimuli in vivo. Neuron. 2012; 74(6):1059–1074. doi:
588 10.1016/j.neuron.2012.04.022.

589 **Bonnevie T**, Dunn B, Fyhn M, Hafting T, Derdikman D, Kubie JL, Roudi Y, Moser EI, Moser MB. Grid cells require
590 excitatory drive from the hippocampus. Nat Neurosci. 2013; 16(3):309–317. doi: 10.1038/nn.3311.

591 **Burgess N**, Barry C, O'Keefe J. An oscillatory interference model of grid cell firing. Hippocampus. 2007;
592 17(9):801–812. doi: 10.1002/hipo.20327.

593 **Bush D**, Burgess N. Neural oscillations: Phase coding in the absence of rhythmicity. Curr Biol. 2019; 29(2):R55–
594 R57. doi: 10.1016/j.cub.2018.11.056.

595 **Buzsáki G**. Theta oscillations in the hippocampus. Neuron. 2002; 33(3):325–340. doi: 10.1016/s0896-
596 6273(02)00586-x.

597 **Buzsáki G**. Neural syntax: Cell assemblies, synapsembles, and readers. Neuron. 2010; 68(3):362–385. doi:
598 10.1016/j.neuron.2010.09.023.

599 **Buzsáki G**, Anastassiou CA, Koch C. The origin of extracellular fields and currents–EEG, ECoG, LFP and spikes.
600 Nat Rev Neurosci. 2012; 13(6):407–20. doi: 10.1038/nrn3241.

601 **Chung JE**, Sellers KK, Leonard MK, Gwilliams L, Xu D, Dougherty ME, Kharazia V, Metzger SL, Welkenhuysen M,
602 Dutta B, Chang EF. High-density single-unit human cortical recordings using the Neuropixels probe. Neuron.
603 2022; 110(15):2409–2421.e3. doi: 10.1016/j.neuron.2022.05.007.

604 **Dehnen G**, Kehl MS, Darcher A, Müller TT, Macke JH, Borger V, Surges R, Mormann F. Duplicate detection of spike
605 events: A relevant problem in human single-unit recordings. Brain Sci. 2021; 11(6):761. doi: 10.3390/brain-
606 sci11060761.

607 **Despouy E**, Curot J, Reddy L, Nowak LG, Deudon M, Sol JC, Lotterie JA, Denuelle M, Maziz A, Bergaud C, Thorpe SJ,
608 Valton L, Barbeau EJ. Recording local field potential and neuronal activity with tetrodes in epileptic patients.
609 J Neurosci Methods. 2020; 341:108759. doi: 10.1016/j.jneumeth.2020.108759.

610 **Donoghue T**, Haller M, Peterson EJ, Varma P, Sebastian P, Gao R, Noto T, Lara AH, Wallis JD, Knight RT, Shestyuk
611 A, Voytek B. Parameterizing neural power spectra into periodic and aperiodic components. Nat Neurosci.
612 2020; 23(12):1655–1665. doi: 10.1038/s41593-020-00744-x.

613 **Donoghue T**, Schaworonkow N, Voytek B. Methodological considerations for studying neural oscillations. Eur
614 J Neurosci. 2022; 55(11-12):3502–3527. doi: 10.1111/ejn.15361.

615 **Eichenbaum H**. A cortical–hippocampal system for declarative memory. Nat Rev Neurosci. 2000; 1(1):41–50.
616 doi: 10.1038/35036213.

617 **Ekstrom AD**, Kahana MJ, Caplan JB, Fields TA, Isham EA, Newman EL, Fried I. Cellular networks underlying
618 human spatial navigation. Nature. 2003; 425(6954):184–188. doi: 10.1038/nature01964.

619 **Ekstrom AD**, Caplan JB, Ho E, Shattuck K, Fried I, Kahana MJ. Human hippocampal theta activity during virtual
620 navigation. Hippocampus. 2005; 15(7):881–889. doi: 10.1002/hipo.20109.

621 **Eliav T**, Geva-Sagiv M, Yartsev MM, Finkelstein A, Rubin A, Las L, Ulanovsky N. Nonoscillatory phase cod-
622 ing and synchronization in the bat hippocampal formation. Cell. 2018; 175(4):1119–1130.e15. doi:
623 10.1016/j.cell.2018.09.017.

624 **Fell J**, Axmacher N. The role of phase synchronization in memory processes. Nat Rev Neurosci. 2011; 12(2):105–
625 118. doi: 10.1038/nrn2979.

626 **Fernández-Ruiz A**, Oliva A, Nagy GA, Maurer AP, Berényi A, Buzsáki G. Entorhinal-CA3 dual-input control
627 of spike timing in the hippocampus by theta-gamma coupling. Neuron. 2017; 93(5):1213–1226.e5. doi:
628 10.1016/j.neuron.2017.02.017.

629 **Fried I**, Wilson CL, Maidment NT, Engel Jr J, Behnke E, Fields TA, Macdonald KA, Morrow JW, Ackerson L. Cerebral
630 microdialysis combined with single-neuron and electroencephalographic recording in neurosurgical patients.
631 J Neurosurg. 1999; 91(4):697–705. doi: 10.3171/jns.1999.91.4.0697.

632 **Fries P**. A mechanism for cognitive dynamics: Neuronal communication through neuronal coherence. Trends
633 Cogn Sci. 2005; 9(10):474–480. doi: 10.1016/j.tics.2005.08.011.

634 **Fujisawa S**, Buzsáki G. A 4 Hz oscillation adaptively synchronizes prefrontal, VTA, and hippocampal activities.
635 Neuron. 2011; 72(1):153–165. doi: 10.1016/j.neuron.2011.08.018.

636 **Goyal A**, Miller J, Qasim SE, Watrous AJ, Zhang H, Stein JM, Inman CS, Gross RE, Willie JT, Lega B, Lin JJ, Sharan
637 A, Wu C, Sperling MR, Sheth SA, McKhann GM, Smith EH, Schevon C, Jacobs J. Functionally distinct high and
638 low theta oscillations in the human hippocampus. Nat Commun. 2020; 11(1):2469. doi: 10.1038/s41467-020-
639 15670-6.

640 **Hasselmo ME**. What is the function of hippocampal theta rhythm? - Linking behavioral data to phasic proper-
641 ties of field potential and unit recording data. Hippocampus. 2005; 15(7):936–949. doi: 10.1002/hipo.20116.

642 **Herweg NA**, Solomon EA, Kahana MJ. Theta oscillations in human memory. Trends Cogn Sci. 2020; 24(3):208–
643 227. doi: 10.1016/j.tics.2019.12.006.

644 **Huerta PT**, Lisman JE. Bidirectional synaptic plasticity induced by a single burst during cholinergic theta oscil-
645 lation in CA1 in vitro. Neuron. 1995; 15(5):1053–1063. doi: 10.1016/0896-6273(95)90094-2.

646 **Hyman JM**, Wyble BP, Goyal V, Rossi CA, Hasselmo ME. Stimulation in hippocampal region CA1 in behaving rats
647 yields long-term potentiation when delivered to the peak of theta and long-term depression when delivered
648 to the trough. J Neurosci. 2003; 23(37):11725–31. doi: 10.1523/JNEUROSCI.23-37-11725.2003.

649 **Hyman JM**, Zilli EA, Paley AM, Hasselmo ME. Medial prefrontal cortex cells show dynamic modulation
650 with the hippocampal theta rhythm dependent on behavior. Hippocampus. 2005; 15(6):739–749. doi:
651 10.1002/hipo.20106.

652 **Hyman JM**, Zilli EA, Paley AM, Hasselmo ME. Working memory performance correlates with prefrontal-
653 hippocampal theta interactions but not with prefrontal neuron firing rates. Front Integr Neurosci. 2010;
654 4:2. doi: 10.3389/neuro.07.002.2010.

655 **Ito HT**, Moser EI, Moser MB. Supramammillary nucleus modulates spike-time coordination in the
656 prefrontal-thalamo-hippocampal circuit during navigation. Neuron. 2018; 99(3):576–587.e5. doi:
657 10.1016/j.neuron.2018.07.021.

658 **Jacobs J**, Kahana MJ, Ekstrom AD, Fried I. Brain oscillations control timing of single-neuron activity in humans.
659 J Neurosci. 2007; 27(14):3839–3844. doi: 10.1523/JNEUROSCI.4636-06.2007.

660 **Jacobs J**, Kahana MJ, Ekstrom AD, Mollison MV, Fried I. A sense of direction in human entorhinal cortex. Proc
661 Natl Acad Sci U S A. 2010; 107(14):6487–6492. doi: 10.1073/pnas.0911213107.

662 **Jones MW**, Wilson MA. Theta rhythms coordinate hippocampal-prefrontal interactions in a spatial memory
663 task. PLoS Biol. 2005; 3(12):e402. doi: 10.1371/journal.pbio.0030402.

664 **Kamiński J**, Brzezicka A, Mamelak AN, Rutishauser U. Combined phase-rate coding by persistently active
665 neurons as a mechanism for maintaining multiple items in working memory in humans. Neuron. 2020;
666 106(2):256–264.e3. doi: 10.1016/j.neuron.2020.01.032.

667 **Kamondi A**, Acsády L, Wang XJ, Buzsáki G. Theta oscillations in somata and dendrites of hippocampal pyramidal
668 cells in vivo: activity-dependent phase-precession of action potentials. Hippocampus. 1998; 8(3):244–261.
669 doi: 10.1002/(SICI)1098-1063(1998)8:3<244::AID-HIPO7>3.0.CO;2-J.

670 **Kocsis B**, Vertes RP. Dorsal raphe neurons: synchronous discharge with the theta rhythm of the hippocampus
671 in the freely behaving rat. J Neurophysiol. 1992; 68(4):1463–1467. doi: 10.1152/jn.1992.68.4.1463.

672 **Kunz L**, Wang L, Lachner-Piza D, Zhang H, Brandt A, Dümpelmann M, Reinacher PC, Coenen VA, Chen D, Wang
673 WX, Zhou W, Liang S, Grewe P, Bien CG, Bierbrauer A, Schröder TN, Schulze-Bonhage A, Axmacher N. Hip-
674 pocampal theta phases organize the reactivation of large-scale electrophysiological representations during
675 goal-directed navigation. Sci Adv. 2019; 5(7):eaav8192. doi: 10.1126/sciadv.aav8192.

676 **Lega BC**, Jacobs J, Kahana M. Human hippocampal theta oscillations and the formation of episodic memories.
677 Hippocampus. 2012; 22(4):748–761. doi: 10.1002/hipo.20937.

678 **Manning JR**, Jacobs J, Fried I, Kahana MJ. Broadband shifts in local field potential power spectra are correlated
679 with single-neuron spiking in humans. J Neurosci. 2009; 29(43):13613–13620. doi: 10.1523/JNEUROSCI.2041-
680 09.2009.

681 **Minxha J**, Adolphs R, Fusi S, Mamelak AN, Rutishauser U. Flexible recruitment of memory-based choice rep-
682 resentations by the human medial frontal cortex. Science. 2020; 368(6498):eaba3313. doi: 10.1126/sci-
683 ence.aba3313.

684 **Minxha J**, Mosher C, Morrow JK, Mamelak AN, Adolphs R, Gothard KM, Rutishauser U. Fixations gate species-
685 specific responses to free viewing of faces in the human and macaque amygdala. Cell Rep. 2017; 18(4):878–
686 891. doi: 10.1016/j.celrep.2016.12.083.

687 **Moscovitch M**, Cabeza R, Winocur G, Nadel L. Episodic memory and beyond: The hippocampus and neocortex
688 in transformation. Annu Rev Psychol. 2016; 67:105–134. doi: 10.1146/annurev-psych-113011-143733.

689 **North BV**, Curtis D, Sham PC. A note on the calculation of empirical P values from Monte Carlo procedures.
690 Am J Hum Genet. 2002; 71(2):439–41. doi: 10.1086/341527.

691 **O'Keefe J**, Burgess N. Dual phase and rate coding in hippocampal place cells: Theoretical significance and
692 relationship to entorhinal grid cells. Hippocampus. 2005; 15(7):853–866. doi: 10.1002/hipo.20115.

693 **Padilla-Coreano N**, Canetta S, Mikofsky RM, Alway E, Passecker J, Myroshnychenko MV, Garcia-Garcia AL, War-
694 ren R, Teboul E, Blackman DR, Morton MP, Hupalo S, Tye KM, Kellendonk C, Kupferschmidt DA, Gordon JA.
695 Hippocampal-prefrontal theta transmission regulates avoidance behavior. Neuron. 2019; 104(3):601–610.e4.
696 doi: 10.1016/j.neuron.2019.08.006.

697 **Pavlides C**, Greenstein YJ, Grudman M, Winson J. Long-term potentiation in the dentate gyrus is induced pref-
698 erentially on the positive phase of theta-rhythm. Brain Research. 1988; 439(1-2):383–387. doi: 10.1016/0006-
699 8993(88)91499-0.

700 **Penner C**, Minxha J, Chandravadia N, Mamelak AN, Rutishauser U. Properties and hemispheric differences of
701 theta oscillations in the human hippocampus. Hippocampus. 2022; 32(5):335–341. doi: 10.1002/hipo.23412.

702 **Qasim SE**, Fried I, Jacobs J. Phase precession in the human hippocampus and entorhinal cortex. Cell. 2021;
703 184(12):3242–3255.e10. doi: 10.1016/j.cell.2021.04.017.

704 **Quiroga RQ**, Nadasdy Z, Ben-Shaul Y. Unsupervised spike detection and sorting with wavelets and superpara-
705 magnetic clustering. Neural Comput. 2004; 16(8):1661–1687. doi: 10.1162/089976604774201631.

706 **Rajasethupathy P**, Sankaran S, Marshel JH, Kim CK, Ferenczi E, Lee SY, Berndt A, Ramakrishnan C, Jaffe A, Lo M,
707 Liston C, Deisseroth K. Projections from neocortex mediate top-down control of memory retrieval. Nature.
708 2015; 526(7575):653–659. doi: 10.1038/nature15389.

709 **Ranganath C**, Ritchey M. Two cortical systems for memory-guided behaviour. Nat Rev Neurosci. 2012;
710 13(10):713–26. doi: 10.1038/nrn3338.

711 **Ray S**. Challenges in the quantification and interpretation of spike-LFP relationships. Curr Opin Neurobiol.
712 2015; 31:111–118. doi: 10.1016/j.conb.2014.09.004.

713 **Reed CM**, Mosher CP, Chandravadia N, Chung JM, Mamelak AN, Rutishauser U. Extent of single-neuron activ-
714 ity modulation by hippocampal interictal discharges predicts declarative memory disruption in humans. J
715 Neurosci. 2020; 40(3):682–693. doi: 10.1523/JNEUROSCI.1380-19.2019.

716 **Rutishauser U**, Ross IB, Mamelak AN, Schuman EM. Human memory strength is predicted by theta-frequency
717 phase-locking of single neurons. Nature. 2010; 464(7290):903–907. doi: 10.1038/nature08860.

718 **Schonhaut DR**, Aghajan ZM, Kahana MJ, Fried I. A neural code for spatiotemporal context. bioRxiv. 2022; doi:
719   10.1101/2022.05.10.491339.

720 **Siapas AG**, Lubenov EV, Wilson MA. Prefrontal phase locking to hippocampal theta oscillations. Neuron. 2005;
721   46(1):141–151. doi: 10.1016/j.neuron.2005.02.028.

722 **Sirota A**, Montgomery S, Fujisawa S, Isomura Y, Zugaro M, Buzsáki G. Entrainment of neocortical neu-
723   rons and gamma oscillations by the hippocampal theta rhythm. Neuron. 2008; 60(4):683–697. doi:
724   10.1016/j.neuron.2008.09.014.

725 **Skelin I**, Zhang H, Zheng J, Ma S, Mander BA, McManus OK, Vadera S, Knight RT, McNaughton BL, Lin JJ. Coupling
726   between slow waves and sharp-wave ripples engages distributed neural activity during sleep in humans. Proc
727   Natl Acad Sci U S A. 2021; 118(21):e2012075118. doi: 10.1073/pnas.2012075118.

728 **Solomon EA**, Kragel JE, Sperling MR, Sharan A, Worrell G, Kucewicz M, Inman CS, Lega B, Davis KA, Stein JM,
729   Jobst BC, Zaghloul KA, Sheth SA, Rizzuto DS, Kahana MJ. Widespread theta synchrony and high-frequency
730   desynchronization underlies enhanced cognition. Nat Commun. 2017; 8(1):1704. doi: 10.1038/s41467-017-
731   01763-2.

732 **Squire LR**. Memory: Neural organization and behavior. In: *Comprehensive Physiology* John Wiley Sons, Ltd;
733   2011.p. 295–371. doi: 10.1002/cphy.cp010508.

734 **Stangl M**, Topalovic U, Inman CS, Hiller S, Villaroman D, Aghajan ZM, Christov-Moore L, Hasulak NR, Rao VR,
735   Halpern CH, Eliashiv D, Fried I, Suthana N. Boundary-anchored neural mechanisms of location-encoding for
736   self and others. Nature. 2021; 589(7842):420–425. doi: 10.1038/s41586-020-03073-y.

737 **Strange BA**, Witter MP, Lein ES, Moser EI. Functional organization of the hippocampal longitudinal axis. Nat
738   Rev Neurosci. 2014; 15(10):655–669. doi: 10.1038/nrn3785.

739 **Trimper JB**, Colgin LL. Spike time synchrony in the absence of continuous oscillations. Neuron. 2018;
740   100(3):527–529. doi: 10.1016/j.neuron.2018.10.036.

741 **Vass LK**, Copara MS, Seyal M, Shahlaie K, Farias ST, Shen PY, Ekstrom AD. Oscillations go the distance: Low-
742   frequency human hippocampal oscillations code spatial distance in the absence of sensory cues during tele-
743   portation. Neuron. 2016; 89(6):1180–1186. doi: 10.1016/j.neuron.2016.01.045.

744 **Watrous AJ**, Fried I, Ekstrom AD. Behavioral correlates of human hippocampal delta and theta oscillations
745   during navigation. J Neurophysiol. 2011; 105(4):1747–1755. doi: 10.1152/jn.00921.2010.

746 **Watrous AJ**, Lee DJ, Izadi A, Gurkoff GG, Shahlaie K, Ekstrom AD. A comparative study of human and rat hip-
747   pocampal low-frequency oscillations during spatial navigation. Hippocampus. 2013; 23(8):656–661. doi:
748   10.1002/hipo.22124.

749 **Watrous AJ**, Miller J, Qasim SE, Fried I, Jacobs J. Phase-tuned neuronal firing encodes human contextual repre-
750   sentations for navigational goals. eLife. 2018; 7:e32554. doi: 10.7554/eLife.32554.

751 **Watrous AJ**, Tandon N, Conner CR, Pieters T, Ekstrom AD. Frequency-specific network connectivity increases un-
752   derlie accurate spatiotemporal memory retrieval. Nat Neurosci. 2013; 16(3):349–356. doi: 10.1038/nn.3315.

753 **Whitten TA**, Hughes AM, Dickson CT, Caplan JB. A better oscillation detection method robustly extracts EEG
754   rhythms across brain state changes: The human alpha rhythm as a test case. Neuroimage. 2011; 54(2):860–
755   874. doi: 10.1016/j.neuroimage.2010.08.064.

756 **Yadav N**, Noble C, Niemeyer JE, Terceros A, Victor J, Liston C, Rajasethupathy P. Prefrontal feature representa-
757   tions drive memory recall. Nature. 2022; 608(7921):153–160. doi: 10.1038/s41586-022-04936-2.

758 **Zhang H**, Jacobs J. Traveling theta waves in the human hippocampus. J Neurosci. 2015; 35(36):12477–12487.
759   doi: 10.1523/JNEUROSCI.5102-14.2015.

760 **Zheng J**, Stevenson RF, Mander BA, Mnatsakanyan L, Hsu FPK, Vadera S, Knight RT, Yassa MA, Lin JJ. Multiplexing
761   of theta and alpha rhythms in the amygdala-hippocampal circuit supports pattern separation of emotional
762   information. Neuron. 2019; 102(4):887–898.e5. doi: 10.1016/j.neuron.2019.03.025.
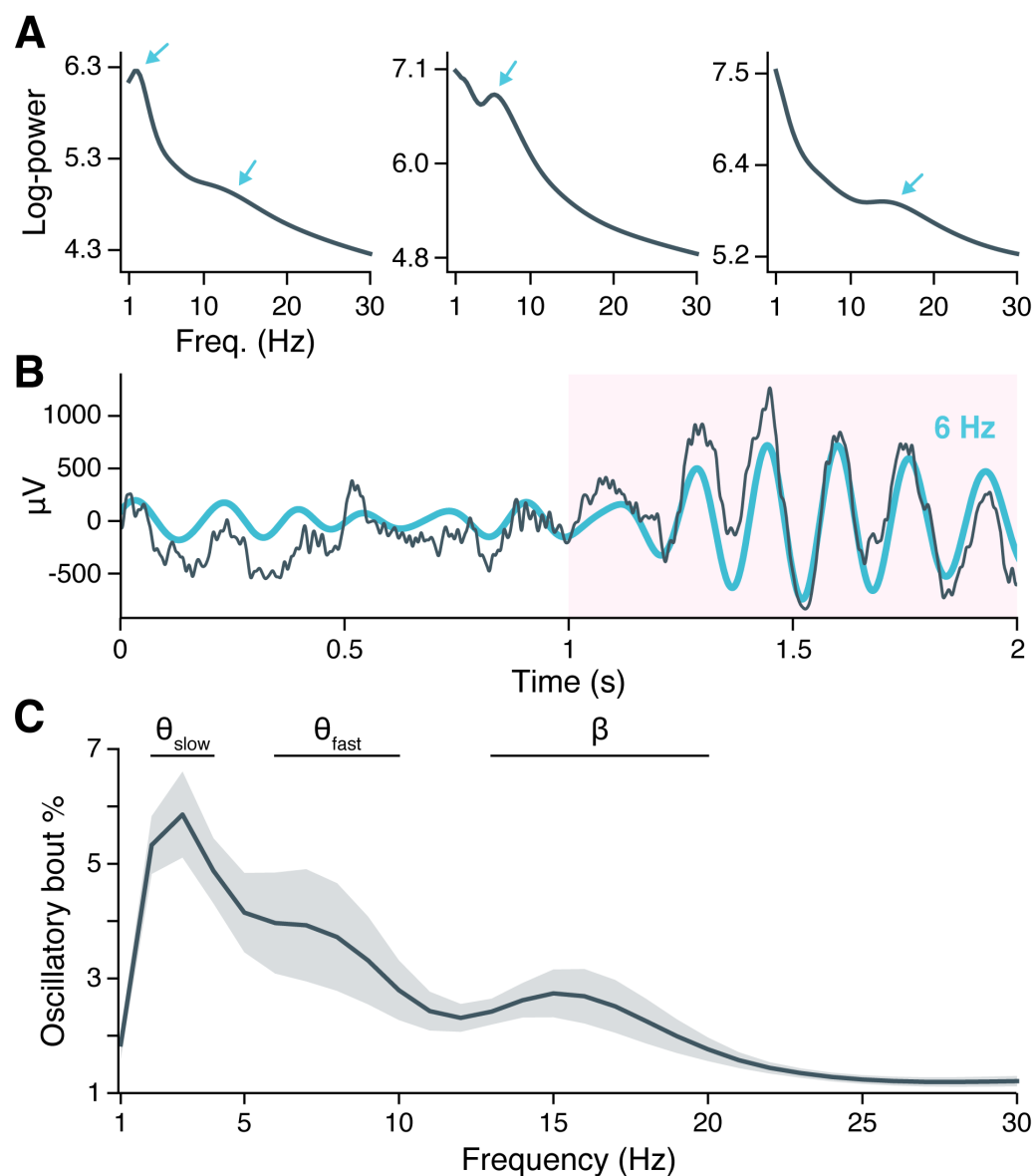
Figure 1. Neural oscillations in the hippocampus. (**A**) Spectral power across the recording session is shown for hippocampal LFPs from three example subjects. Arrows indicate spectral peaks above the background 1/f spectrum. (**B**) A hippocampal LFP trace (gray line = raw LFP, cyan line = 6Hz filtered LFP) is shown immediately before and during a BOSC-detected theta oscillation, highlighted in pink. (**C**) Mean ± SEM percent time, across subjects, that BOSC-detected oscillations were present in hippocampal LFPs at each frequency from 1-30Hz.
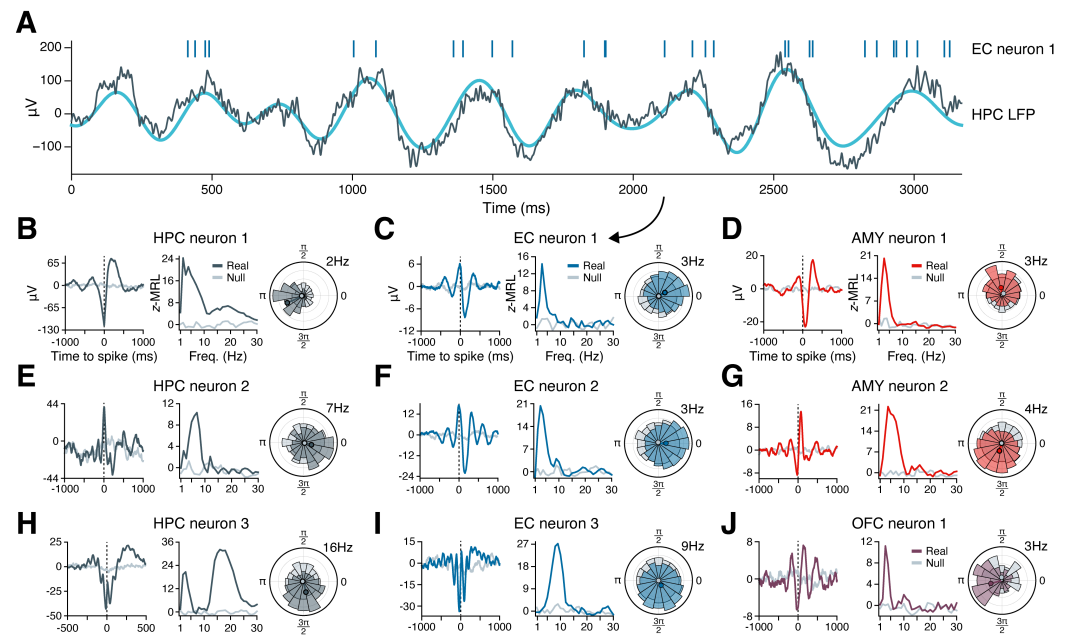
Figure 2. Example phase-locking to hippocampal oscillations. (**A**) Spikes from an EC neuron (top, vertical lines) are shown alongside LFP activity in the hippocampus during a slow theta oscillation (gray line = raw LFP, cyan line = 3Hz filtered LFP). Panel (C) shows phase-locking statistics for this neuron across the recording session. (**B-J**) Shown are nine neurons in the HPC (left column), EC (middle column), AMY (right column, top two rows), and OFC (right column, bottom row) that phase-locked to oscillatory signals in the hippocampus while subjects navigated through a virtual environment. The left subpanel for each neuron shows the mean hippocampal LFP centered on the time of each spike. The middle subpanel shows the phase-locking strength at each frequency relative to a null distribution of circularly-shifted spikes. The right subpanel shows the spike-phase distribution at the maximum phase-locking frequency. Dark gray (HPC), blue (EC), red (AMY) and purple (OFC) lines correspond to true spike times, while light gray lines correspond to circularly-shifted spike times from a single draw from the null distribution. HPC = hippocampus; EC = entorhinal cortex; AMY = amygdala; OFC = orbitofrontal cortex.
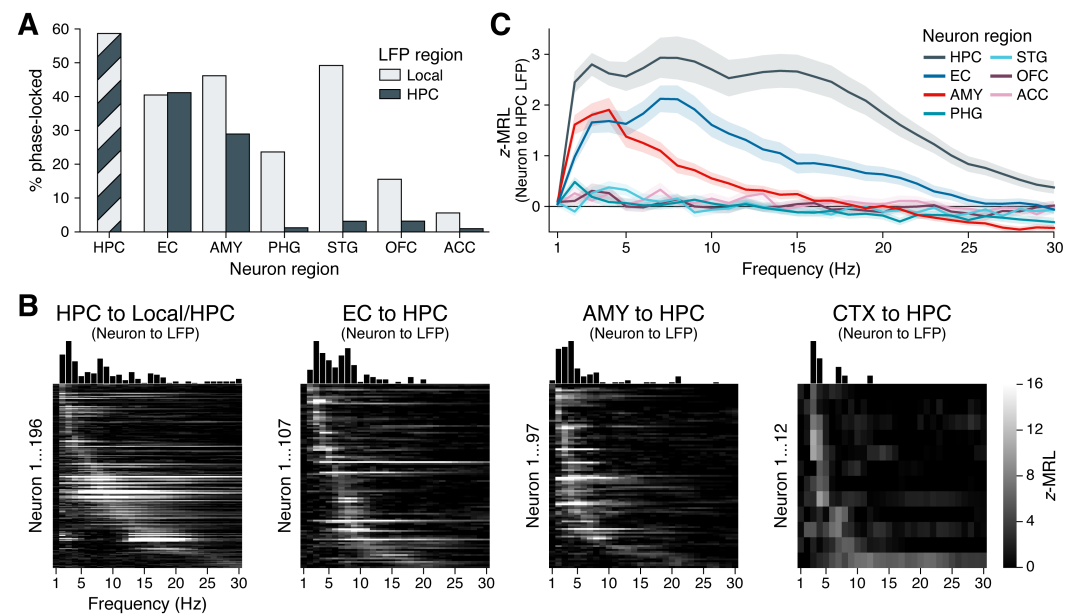
Figure 3. Phase-locking to hippocampal oscillations by region and frequency. (**A**) Bars show the percentage of neurons in each region that phase-locked to locally-recorded LFP oscillations (light gray) and hippocampal LFP oscillations (dark gray). (Note that local and hippocampal LFP is identical for hippocampal neurons.) Phase-locking significance was set at FDR-corrected $p < 0.05$ within each bar group. (**B**) Heatmaps show the phase-locking strength (z-MRL; color scale intensity) by hippocampal LFP oscillation frequency (x-axis) for all significantly phase-locked neurons (y-axis; each row = one neuron) in the HPC, EC, AMY, and remaining regions (CTX), respectively. Neurons in each region are sorted from top to bottom by frequency of maximum phase-locking strength. Neurons depicted match the dark gray bars in (A). (**C**) Mean ± SEM phase-locking strength by hippocampal oscillation frequency is shown for all neurons in each region, regardless of their individual phase-locking significance as depicted in (A) and (B). HPC = hippocampus; EC = entorhinal cortex; AMY = amygdala; PHG = parahippocampal gyrus; STG = superior temporal gyrus; OFC = orbitofrontal cortex; ACC = anterior cingulate cortex.
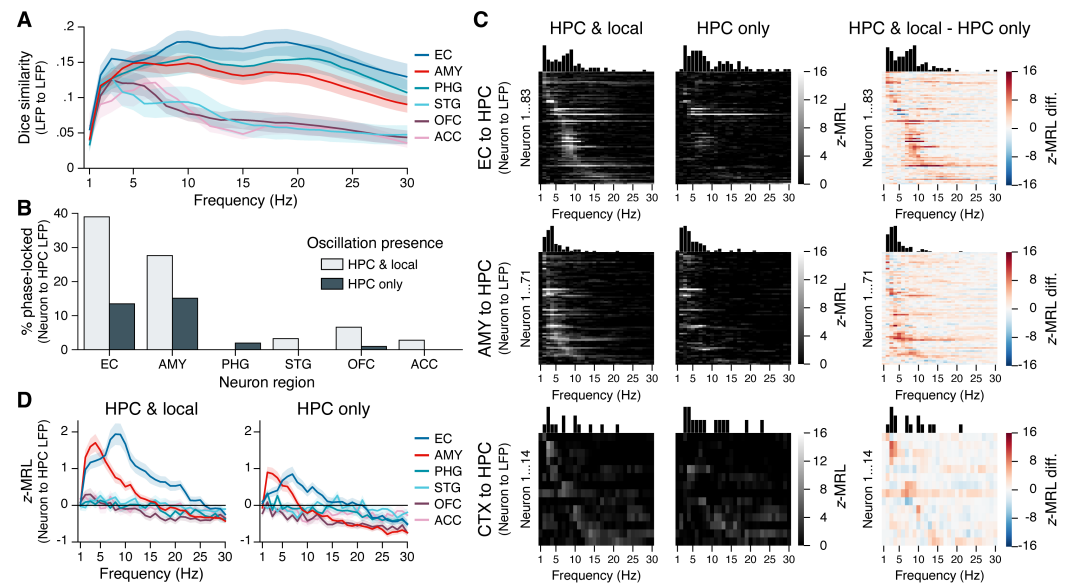
Figure 4. Phase-locking to hippocampal oscillations with and without co-occurring local oscillations.
(**A**) Mean ± SEM Dice coefficient across subjects shows the percent overlap between oscillatory bouts in the hippocampus and in each extrahippocampal region. (**B**) Bars show the percentage of neurons in each region that phase-locked to hippocampal oscillations when local oscillations were present (light gray) or absent (dark gray). Phase-locking significance was set at FDR-corrected $p < 0.05$ within each bar group. (**C**) Heatmaps show the phase-locking strength by hippocampal LFP oscillation frequency for all significantly phase-locked neurons in the EC (top row), AMY (middle row), and remaining regions (CTX; bottom row), when hippocampal and local oscillations co-occurred (left column) versus when only hippocampal oscillations occurred (middle column). The right column shows the left column minus middle column values. Neurons in each region are sorted from top to bottom by frequency with the maximum phase-locking strength, and the sorting order is constant across columns within each row. Neurons depicted match the union of light gray and dark gray bars in (B). (**D**) Phase-locking to the hippocampus is shown during co-occurring local and hippocampal oscillations (left) or only hippocampal oscillations (right). Each subpanel shows the mean ± SEM phase-locking strength by hippocampal oscillation frequency for all neurons in each region, regardless of their individual phase-locking significance as depicted in (B) and (C). HPC = hippocampus; EC = entorhinal cortex; AMY = amygdala; PHG = parahippocampal gyrus; STG = superior temporal gyrus; OFC = orbitofrontal cortex; ACC = anterior cingulate cortex.

Region	Subjects	Neurons	Firing rate (Hz)
Hippocampus	27	391	1.6 (0.6, 4.7)
Entorhinal cortex	19	341	2.3 (1.0, 5.5)
Amygdala	23	439	1.5 (0.6, 3.7)
Parahippocampal gyrus	15	217	2.2 (0.8, 4.5)
Superior temporal gyrus	5	139	3.4 (1.4, 8.6)
Orbitofrontal cortex	15	193	2.0 (0.9, 4.9)
Anterior cingulate cortex	8	134	3.1 (1.4, 6.8)
Total	*28*	*1,854*	*2.0 (0.8, 5.0)*

Table 1. Neurons by region. Table shows how many subjects had 1+ neurons in each brain region, how many neurons were recorded in each region, and the median, lower, and upper quartile firing rates for these neurons.
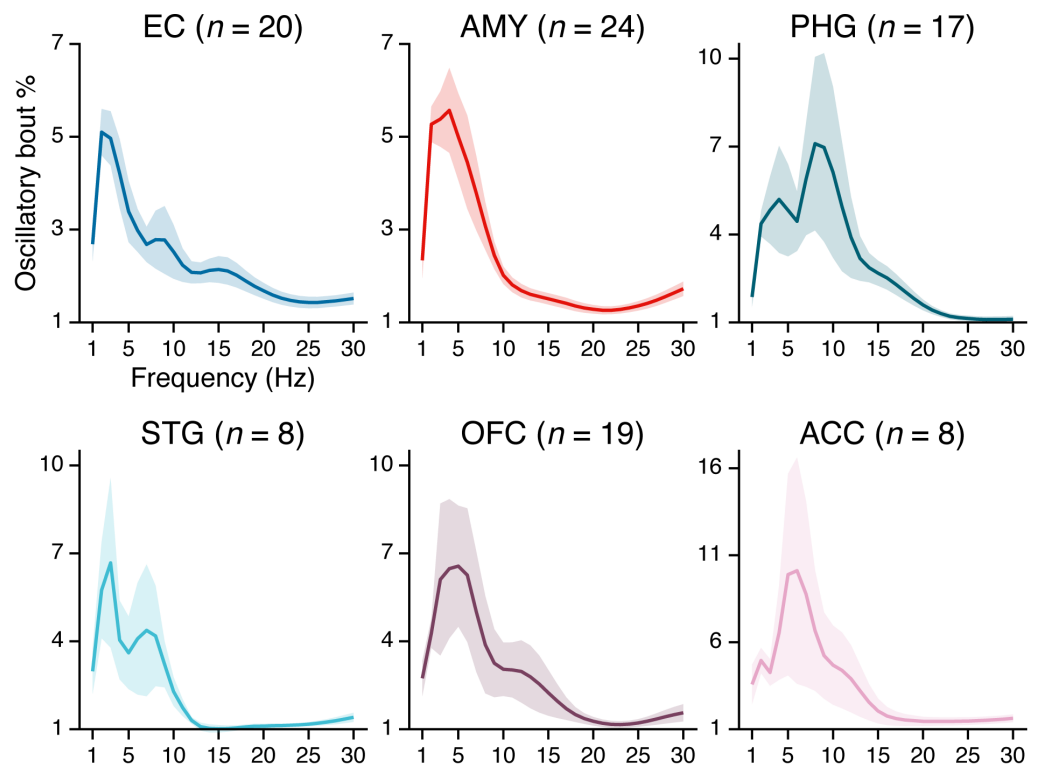
Supplemental figures

Figure 1—figure supplement 5. Neural oscillations outside the hippocampus. Subpanels show the mean ± SEM percent time, across *n* subjects, that BOSC-detected oscillations were present in each region at 1-30Hz frequencies. (Note the differences in y-axis scaling due to higher variance at lower sample sizes.)
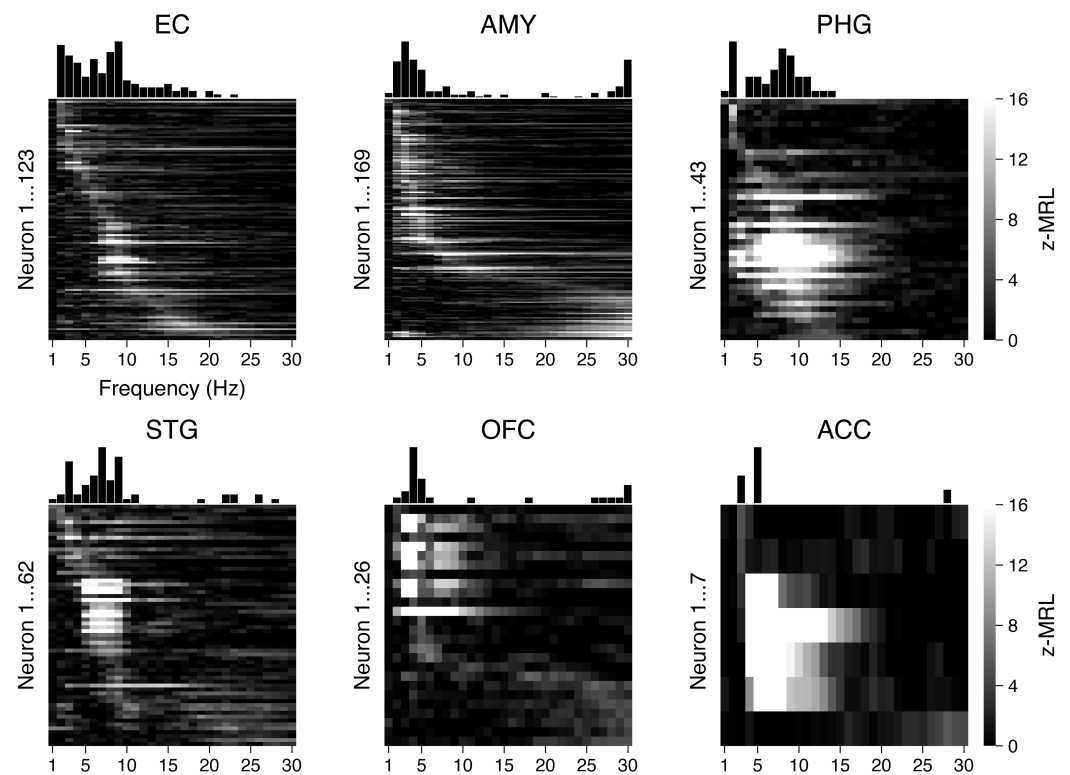
Figure 3—figure supplement 1. Phase-locking to local oscillations. Heatmaps show the phase-locking strength (z-MRL; color scale intensity) by local oscillation frequency (x-axis) for all significantly phase-locked neurons (y-axis; each row = one neuron) in each region, respectively. Neurons in each region are sorted from top to bottom by frequency of maximum phase-locking strength. Neurons depicted match the light gray bars in Figure 3A.
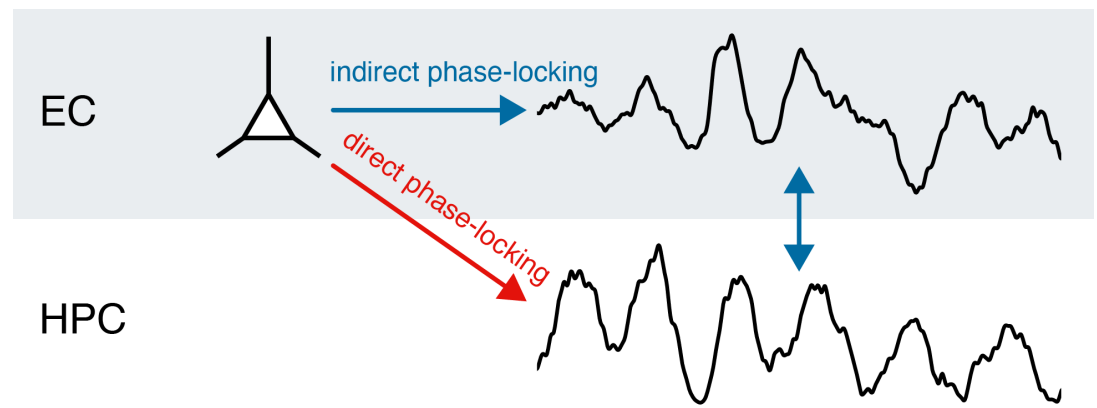
Figure 4—figure supplement 1. Two explanations for remote phase-locking to hippocampal theta.
Figure illustration shows two ways in which phase-locking of extrahippocampal neurons to hippocampal theta could occur. In the first scenario, an EC neuron phase-locks to the local theta rhythm, which in turn exhibits phase-synchrony with hippocampal theta ("indirect phase-locking," blue arrows). In the second scenario, the EC neuron is directly entrained to hippocampal theta, such that phase-locking can occur even absent a local theta rhythm ("direct phase-locking," red arrow).
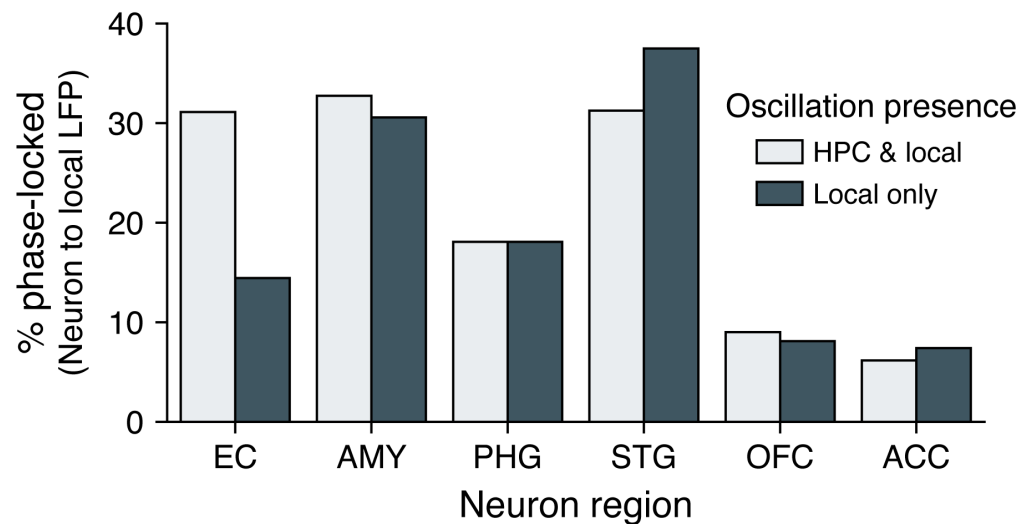
Figure 4—figure supplement 2. Phase-locking to local oscillations with and without co-occurring hippocampal oscillations. Bars show the percentage of neurons in each region that phase-locked to local oscillations when hippocampal oscillations were present (light gray) or absent (dark gray). Phase-locking significance was set at FDR-corrected $p < 0.05$ within each bar group.